Journal of Industrial and Engineering Chemistry 163 (2026) 646–659

Contents lists available at ScienceDirect

Journal of Industrial and Engineering Chemistry

journal homepage: www.elsevier.com/locate/jiec

Photodynamically active Poly(vinyl chloride) material functionalized with zinc phthalocyanine and zinc pyrithione for antibacterial and antiviral performance

Hana Pistekova [a,*], Martina Pummerova [a,*], Monika Strasakova [a], Miroslava Dusankova [a], Martin Novak [a], Radka Korinkova [b], Vojtech Trousil [b], Dominika Hanusova [a], Jakub Sevcik [a], Eva Domincova Bergerova [a], Vladimir Sedlarik [a,*]

[a] Centre of Polymer Systems, University Institute, Tomas Bata University in Zlin, tr., Tomase Bati 5678,760 01 Zlin, Czech Republic
[b] Centre of Organic Chemistry ltd., CZ 533 54 Rybitvi 296, Czech Republic

ARTICLE INFO

Keywords:
Poly(vinyl chloride) (PVC)
Zinc phthalocyanine
Photodynamic antimicrobial materials
Singlet oxygen
Antimicrobial polymer surfaces
Zinc pyrithione

ABSTRACT

Functional polymer surfaces that combine antimicrobial activity with retained processability and physicochemical stability are of growing interest for healthcare and high-contact applications. This study reports a photodynamically active poly(vinyl chloride) (PVC) material functionalized with a methacrylate-modified zinc phthalocyanine photosensitizer (ZnPTC-HEMA) and zinc pyrithione (ZPT), fabricated using industrially relevant melt processing and compression molding methods. The resulting material exhibited efficient singlet oxygen generation even at low ZnPTC-HEMA loadings, with activity approaching saturation at higher concentrations. Under visible light irradiation, the modified PVC surfaces exhibited pronounced antibacterial activity against *Staphylococcus aureus* and achieved more than a 5-log reduction of the enveloped bacteriophage Φ6, whereas the non-enveloped phage ΦX174 remained unaffected. The addition of ZPT further broadened antibacterial efficacy, including under dark conditions. Morphological, spectroscopic, thermal, and mechanical analyses confirmed homogeneous additive incorporation, preservation of the PVC chemical structure, and retention of material integrity at low to moderate additive loadings. Migration studies further demonstrated no detectable release of ZnPTC-HEMA after prolonged aqueous exposure. These results establish phthalocyanine functionalized PVC as a scalable light responsive antimicrobial material in which photoactive functionality can be introduced without compromising key processing and performance characteristics.

Introduction

The development of antimicrobial functional materials has become an important research priority for healthcare and high-contact applications, where contaminated surfaces may contribute to microbial transmission and biofilm formation. Respiratory viral outbreaks, including influenza and COVID-19, have highlighted the need for material-based strategies capable of reducing viral contamination at surfaces and interfaces.[1–3] In addition, viral respiratory infections may predispose patients to secondary bacterial infections, including those most commonly caused by *Staphylococcus aureus* and Streptococcus pneumoniae which further supports the development of materials with combined antiviral and antibacterial functionality.[1,4,5]

The use of polymers in medical devices has risen sharply in recent decades. Among these materials, poly(vinyl chloride) (PVC) remains one of the most widely used polymers in healthcare because of its low cost, flexibility, transparency, and excellent processability. It is commonly used in tubing, blood bags, catheters, intravenous therapy containers, and other medical components. However, the hydrophobic character of PVC can promote microbial adhesion and colonization, particularly in short-term and indwelling medical devices. Therefore, the development of PVC materials with antimicrobial functionality remains an important objective in polymer and interface engineering.[6,7]

Antimicrobial PVC-based materials have previously been developed through chemical modification, blending, and incorporation of inorganic or organic antimicrobial agents.[8–11] For instance, PVC–chitosan conjugates containing Ag nanoparticles exhibited pronounced antibacterial activity and were proposed for biomedical applications.

* Corresponding authors.
E-mail addresses: pistekova@utb.cz (H. Pistekova), pummerova@utb.cz (M. Pummerova), sedlarik@utb.cz (V. Sedlarik).

https://doi.org/10.1016/j.jiec.2026.06.020
Received 10 April 2026; Received in revised form 27 May 2026; Accepted 12 June 2026
Available online 15 June 2026
1226-086X/© 2026 The Author(s). Published by Elsevier B.V. on behalf of The Korean Society of Industrial and Engineering Chemistry. This is an open access article under the CC BY license (http://creativecommons.org/licenses/by/4.0/).

[12] Other approaches include functionalized PVC–chitosan biomaterials [8], PVC/1-vinylimidazole nanocomposites loaded with Ag or Cu nanoparticles [11], thiazole-functionalized PVC nanocomposites [9], Schiff base-modified PVC nanocomposites [10], and PVC formulations containing halo-benzothiazole derivatives or bio-based ester additives. [13] These studies highlight the versatility of PVC as an antimicrobial polymer platform. However, most reported systems rely on conventional biocidal additives, metal nanoparticles, or surface-active chemical modifications, whereas the integration of photodynamically active phthalocyanine photosensitizers into melt-processed PVC remains insufficiently explored.[14,15]

Phthalocyanines (PTCs) represent a promising photoactive compound for antimicrobial material design because of their strong visible/near-infrared absorption, high photostability, structural tunability, and efficient generation of reactive oxygen species, particularly singlet oxygen.[16–19] Zinc phthalocyanines are especially attractive photosensitizers due to their favorable photodynamic properties and accessible chemical modification.[19] Previous studies have demonstrated the antimicrobial potential of phthalocyanine-based systems in cellulose materials, textiles, and fibrous membranes.[14,15,20] PTCs have also been investigated as visible-light-active photocatalysts for self-cleaning and environmental decontamination applications.[21,22] Nevertheless, their incorporation into melt-processable commodity polymers, particularly PVC, remains limited, and studies that systematically relate photoactivity, antimicrobial efficacy, and polymer performance are scarce.

Evaluation of new antimicrobial materials increasingly require both antibacterial and antiviral assessment. Since experiments involving human pathogenic viruses are expensive, technically demanding, and constrained by biosafety requirements, bacteriophages are widely used as practical viral surrogates. Selected phages share relevant structural and physicochemical features with eukaryotic viruses, including envelope presence or absence and resistance to disinfection treatments. In this study, two structurally different tailless bacteriophages were selected: enveloped Pseudomonas phage Φ6 (*Cystoviridae* family) as a surrogate for enveloped viruses and non-enveloped coliphage ΦX174 (*Microviridae* family) as a model for non-enveloped viruses.[23–29]

This study aimed to develop and comprehensively evaluate a PVC-based polymer system with light-activated antimicrobial functionality enabled by phthalocyanine incorporation. The material was assessed for antibacterial activity against representative Gram-positive and Gram-negative bacteria and for antiviral performance against Φ6 and ΦX174, and key material parameters relevant to practical implementation, including additive dispersion, migration resistance, thermal stability, and mechanical performance. Although antiviral polymers and bacteriophage-based antiviral testing have each been reported previously,[30] to the best of our knowledge, this is the first study to integrate a zinc phthalocyanine photosensitizer into a melt-processed PVC matrix and systematically relate singlet oxygen generation and antimicrobial performance to polymer morphology, stability, and mechanical behavior.

Materials and methods

Materials

PVC RB3, a commercially supplied medical-grade plasticized PVC compound based on DEHP-plasticized poly(vinyl chloride), was purchased from ModenPlast Medical Srl (Ubersetto di Fiorano, Italy). According to the supplier, RB3 is intended for medical polymer processing; the detailed material composition is proprietary to the manufacturer. The zinc 2-[3-(phthtalocyaninsulphonamido)propoxy]ethylmetacrylate (ZnPTC-HEMA) was synthesized in the Centre of Organic Chemistry (Rybitví, Czech Republic). Zinc Pyrithione (ZPT) was supported by Alchimica (Prague, Czech Republic). All other chemicals were purchased from Merck (Prague, Czech Republic).

Preparation of ZnPTC-HEMA

ZnPTC-HEMA was prepared by a three-step process (Fig. 1). To begin, 304 mL of chlorosulphonic acid was placed in a 1.5 L flask and cooled to 0 – 5 °C in an ice bath. Then, 100 g (173 mmol) of ZnPTC was added in portions, allowing the temperature to rise to 20 °C. The mixture was stirred at this temperature for 30 min, then heated to 120 °C for 1 h. After cooling to 100 °C, 64 mL of thionyl chloride ($SOCl_2$) was added dropwise, and the mixture was maintained at 100 °C for an additional hour. The reaction mixture was then cooled to 20 °C and poured onto a water–ice mixture. The resulting precipitate was collected by filtration, and the filter cake was washed repeatedly with cold water until no sulfate or chloride ions were detected. The resulting paste of phthalocyanine sulfochloride (Pc-SO_2Cl, 603 g) was stored in a refrigerator.

The paste was analyzed for hydrolyzable chlorine and dry matter content (dried at 80 °C). The dry matter was found to be 20.3 %, and the hydrolyzable chlorine content (calculated based on dry mass) was 8.9 % (the theoretical value for the bis-substituted derivative is 9.14 %).

Next, 593 g of the frozen Pc-SO_2Cl was thoroughly dispersed in 543 mL of cold water, followed by the addition of 39 mL of allylamine (521 mmol). The reaction mixture was heated to 40 °C and stirred for 5 h, then cooled to room temperature and filtered. The filter cake was washed thoroughly with water to remove excess amine and dried at 50 °C, yielding 100 g (80 %) of blue ZnPTC-AA.

Subsequently, 100 g of ZnPTC-AA was vigorously dispersed in 450 mL of cold water. Hydroxyethyl methacrylate (19.8 mL, 163 mmol) was then added under stirring. The pH of the reaction mixture (~7) was adjusted to 11 using 4 M NaOH, after which it was heated at 60 °C for 1.5 h. The mixture was cooled to approximately 25 °C and filtered. The filter cake was washed with 100 mL of water and dried at 50 °C to afford 92 g (76 %) of blue ZnPTC-HEMA.

^{1}H and ^{13}C NMR spectroscopy of the final product was performed in DMSO. The spectra were complex due to the presence of multiple isomers with varying degrees of substitution. Nevertheless, several characteristic signals confirmed the molecular structure. 2,5-Bis(2-ethylhexyl)-3,6-diphenyl-1H,2H,4H,5H-pyrrolo[3,4-c]pyrrole-1,4-dione (DPP) was synthesized following a modified procedure based on Pop et al. (2019), in which K_2CO_3/DMF was employed instead of Cs_2CO_3/CH_3CN.[31]

3,6-Diphenyl-1,4-diketopyrrolo[3,4-c]pyrrole (5.00 g, 17.34 mmol) was suspended in anhydrous DMF (150 mL) under a nitrogen atmosphere. Finely powdered K_2CO_3 (9.60 g, 69.37 mmol) was added, and the resulting heterogeneous mixture was stirred at 125 °C for 1 h. 2-Ethylhexyl bromide (13.4 g, 69.37 mmol) was then added dropwise over 3 h, and the reaction mixture was maintained at 125 °C for an additional 20 h.

After cooling to room temperature, the reaction mixture was poured into excess water to induce precipitation. The resulting solid was collected by vacuum filtration, washed thoroughly with water, and dried under reduced pressure. Purification by recrystallization from hot methanol afforded the target compound as a red solid (1.6 g, 18 % yield).

Sample preparation

Firstly, the PVC compound RB3 polymer masterbatch, plasticized with di-2-ethylhexyl phthalate (DEHP) and ZPT, was processed using a Brabender Plastrograph (Brabender GmbH & Co. KG, Duisburg, Germany) at 50 RPM for 3 min at 150 °C and then set aside for further steps. Secondly, the PVC mixture with the ZnPTC-HEMA additive was melt-compounded under identical conditions for 6 min to achieve a homogenized blend.

A calculated amount of this masterbatch and the PVC-ZnPTC-HEMA blend were then reprocessed using an Xplore MC15 micro-compounder (Xplore Instruments BV, Sittard, The Netherlands) at 150 °C and 100 RPM for 5 min. The final composition of the samples is listed in Table 1.

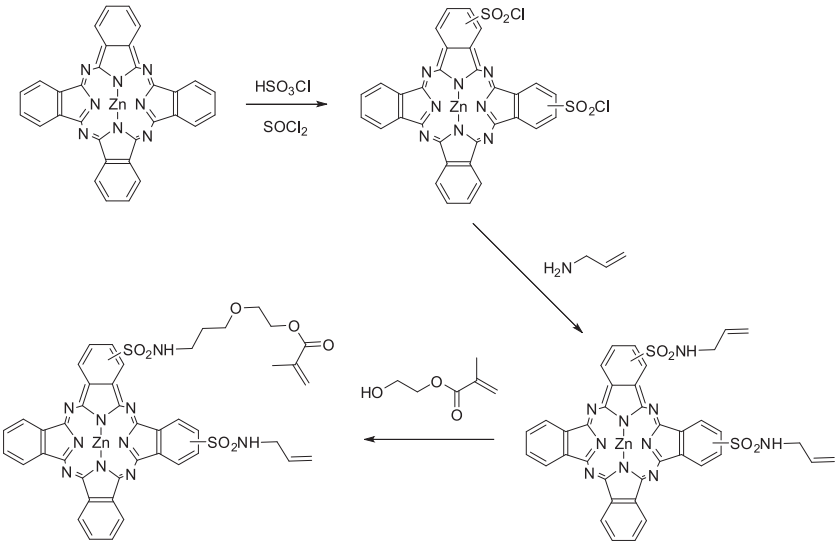


Fig. 1. Synthetic route yielding ZnPTC-HEMA.

Table 1
Quantification of singlet oxygen with varying concentrations of ZnPTC-HEMA.

Sample name	Component (wt %)		
	PVC	ZnPTC-HEMA	ZPT
PVC-0	100	–	–
PVC-0.1	99.9	0.1	–
PVC-0.2	99.8	0.2	–
PVC-0.5	99.5	0.5	–
PVC-1	99.0	1.0	–
PVC-3	97.0	3.0	–
PVC-0-ZPT	100	–	0.005
PVC-0.1-ZPT	99.9	0.1	0.005
PVC-0.2-ZPT	99.8	0.2	0.005
PVC-0.5-ZPT	99.5	0.5	0.005
PVC-1-ZPT	99.0	1.0	0.005
PVC-3-ZPT	97.0	3.0	0.005

For comparison, a reference PVC sample was prepared under the same conditions and with the same instruments.

The final processing step involved compression moulding with a FONTIJNE LabEcon 300 hydraulic press (Fontijne Presses b.v., Rotterdam, The Netherlands) at 150 °C, with an 8-minute tempering period, followed by 3 min of pressing at 200 kN and 3 min of cooling at 400 kN using a Metallkraft WPP 50 M press (Stürmer Maschinen GmbH, Hallstadt, Germany).

Morphology analysis

FEI NanoSEM 450 (FEI Company, The Netherlands) was used to analyse the morphology of PVC samples fracture in order to evaluate the degree of homogeneity. The microscope was operated in vacuum mode at an acceleration volage of 5 kV. The samples were beforehand sputtered with gold and palladium for 30 s.

Chemical structure analysis by Fourier transform infrared spectroscopy (ATR-FTIR) and Nuclear Magnetic Resonance spectroscopy (NMR)

Infrared spectra were recorded using a Nicolet iS5 FTIR spectrometer (Thermo Fisher Scientific, USA) equipped with a diamond ATR crystal. Spectra were collected over the range 4000–400 cm^{-1} at a resolution of 4 cm^{-1}, averaging 64 scans per sample.

^{1}H and ^{13}C NMR spectra of the final ZnPTC-HEMA product were recorded in DMSO-d_6 using a Bruker Avance III HD 500 MHz spectrometer equipped with a PA BBO 500S2 BBF-H-D-05 Z SP probe. ^{1}H NMR spectra were acquired at 500.13 MHz using the zg30 pulse sequence, whereas ^{13}C NMR spectra were acquired at 125.76 MHz using the jmod pulse sequence. For ^{1}H NMR, a spectral width of 10,000 Hz, 64 k data points, 16 scans, and a relaxation delay of 1 s were used. For ^{13}C NMR, a spectral width of 31,250 Hz, 128 k data points, and a relaxation delay of 2 s were applied, with 10,240 scans for ZnPTC-AA and 2,918 scans for ZnPTC-HEMA. Chemical shifts are reported in ppm.

Colorimetric analysis

The colorimetric properties of the PVC samples were analyzed using a UltraScan VIS spectrophotometer (Hunter Lab, USA). The primary analysis utilized the D65/10° spectrum, which simulates daylight at 6500 K, with a viewing angle consistent with the D/8 geometry of the HunterLab Ultrascan instrument.

Thermal properties

The thermal stability and thus the suitability of additives for thermoplastic processing were confirmed using thermogravimetric analysis (TGA). Samples for thermogravimetry measurement were prepared at 8 mg in weight and investigated on a TA Q500 thermogravimetric analyser (TA Instruments, Wilmington, DE, USA) by a TA Universal Analyzer 2000 version 4.5A (TA Instruments – Waters LLC, Wilmington, DE, USA). The instrument was set to a heating rate of 10 °C/min from 25 to 800 °C under a nitrogen atmosphere. Data of initial degradation temperature (T_i), the peak degradation temperature with maximum weight loss rate (T_p), and thermal degradation weight loss of both antimicrobials were collected.

Singlet oxygen quantification

Singlet oxygen production generation was quantified using the 1,3-diphenylisobenzofuran (DPIBF) method in hexan. DPIBF selectively reacts with intermediate singlet oxygen $^{1}O_2$ to form an unstable peroxide that decomposes into the colourless product 1,2-dibenzoylbenzene, enabling specific detection without interference from other reactive oxygen species. Hexane was selected as the solvent because it dissolves DPIBF while leaving PVC and ZnPTC-HEMA insoluble, and it provides a higher molar oxygen solubility compared to water.

Polymer samples were cut into 8 × 8 mm squares, accurately weighed, and placed at the bottom of a spectrophotometer cuvette. Subsequently, 2 mL of hexane and DPIBF (c ≈ 2 g/L) were added to

reach absorbance λ = 417 nm in the range 0.7–0.8. The samples were irradiated with a 661 nm laser (40 mW, focused beam), and the decrease in absorbance at 417 nm was monitored to follow the reaction kinetics. The rate constant **k** (J^{-1}), proportional to $^1O_2$ generation, was determined from the absorbance decay as a function of incident light energy. From these slopes, the indicator half-life values (τ 1/2, s) were calculated for each sample.[32]

Antimicrobial assays

.

Antibacterial efficacy

The antibacterial efficacy of the investigated samples was evaluated under laboratory conditions using standardized test microorganisms and procedures, as detailed below. Before antibacterial testing, samples and polypropylene foils were disinfected by rinsing with 70 % denatured ethanol. For the determination two bacterial strains were used, Gram-negative *Escherichia coli* CCM 4517, equivalent to ATCC 8739, and Gram-positive *Staphylococcus aureus* CCM 4516, equivalent to ATCC 6538, were obtained from the Czech Collection of Microorganisms. *S. aureus* CCM 4516 was selected instead of CCM 2022, equivalent to ATCC 6538P, because preliminary illuminated control experiments showed that CCM 2022 was sensitive to the applied blue-primary LED illumination, whereas CCM 4516 maintained stable viable counts under the same conditions. This enabled a more reliable evaluation of the photoactivated antibacterial effect of the ZnPTC-HEMA-containing PVC materials. These bacteria were selected as model microorganisms because they represent environmentally relevant species. The antibacterial testing was performed according to ISO 22196 with modifications. Bacterial suspensions (*Escherichia coli* $3{,}4{\cdot}10^5$ CFU/mL; *Staphylococcus aureus* $1{,}2{\cdot}10^5$ CFU/mL) were prepared in 500x diluted Nutrient broth (NB, HiMedia laboratories, India). The bacterial suspension was dispensed on the sample surface (dimensions 25 × 25 mm) in the volume 100 μL and the sample was covered with the polypropylene foil (dimensions 20 × 20 mm). Samples with foils were cultivated at 35 °C and ≥ 90 % relative humidity for 18 h. The samples for illumination were incubated in a polymethylmethacrylate incubator with transparent walls and illuminated from a distance of 200 cm by an artificial daylight source (LED source: blue primary emitter 450 nm; Illumination intensity = 1250 lx). After the incubation time, polypropylene foil was removed and each sample was completely washed by Soybean Casein Digest Lecithin Polysorbate broth (SCDLP) broth (HiMedia laboratories, India), which was subsequently collected. The viable bacteria count was determined by the pour plate culture method using Plate Count Agar (PCA, HiMedia laboratories, India). After the incubation, the number of bacteria colonies in the Petri dishes was determined. Neat PVC without active additives, designated as PVC-0 and prepared under identical processing conditions, was used as the reference sample for calculation of antibacterial activity.

The antibacterial activity (R) was calculated using Equation (1):

$$R = \log N_{blank} - \log N_{sample}, \quad (1)\ .$$

where $\log N_{blank}$ and $\log N_{sample}$ are the logarithms of viable bacteria number in the reference and modified sample, respectively. All experiments were conducted in triplicate, with a minimum of two independent determinations for each parameter.

Statistical significance was evaluated by applying one-way ANOVA ($P < 0.05$); (OriginPro 2024, OriginLab Corporation, Massachusetts, USA); experimental data are reported as the mean values of three replicates ± standard deviation.

Antiviral efficacy

In this work, bacteriophages Pseudomonas phage Φ6 DSM 21518, Escherichia phage ΦX174 DSM 4497 and their host cultures Pseudomonas syringae DSM 21518 and *Escherichia coli* DSM 13127 were sourced from Leibniz Institute DSMZ-German collection of Microorganisms and Cell Culture GmbH (Braunschweig, Germany). The received microorganisms were cultured following the manufacturer's instructions. Stock cultures of P. syringae and *E. coli* were stored at −70 °C, whilst the Φ6 and ΦX174 bacteriophages were stored in refrigerator at 4 °C.

The antiviral activity of the samples was compared to neat PVC without active substances in a polymer matrix and were performed according to a modified ISO 22196:2021 standard. A phage lysate with an initial viral particle concentration of approximately 10^9 PFU/mL, prepared according to the supplier's instructions, was diluted 500-fold in NB (HiMedia Laboratories, India) to obtain viral suspensions with final concentrations of Φ6 (1.8×10^6 PFU/mL) and ΦX174 (7.7×10^6 PFU/mL). Samples were incubated with the respective viral suspensions for 18 h. Incubation was carried out according to the preferences of the host culture: 25 °C for phage Φ6 and 35 °C for ΦX174 and relative humidity ≥ 90 %. After rinsing the samples, phage was assayed by the double layer method, when phage suspension (0.1 mL) was mixed with 0.1 mL host culture (OD = 0.3) and 3 mL top agar and poured on to surface of a bottom agar plate. Disinfection of the samples, methodology, sample dimensions and calculation of antiviral activity were the same as for bacteria. Thus, compared with ISO 22196, the main modifications were: i) the use of bacteriophages instead of bacteria, ii) host-specific incubation conditions, iii) quantification of infectious particles by PFU-based plaque assay rather than CFU-based colony counting, and iv) calculation of antiviral activity from the logarithmic reduction in infectious phage titer relative to the PVC-0 reference sample. Sample dimensions, polypropylene cover film dimensions, disinfection procedure, contact time, high-humidity incubation, and the general log-reduction calculation followed the same surface-contact framework as used for the antibacterial assay.

Migration study

Migration testing was carried out according to ČSN EN 1186 (Migration from plastics into food simulants). Prior to testing, PVC foils containing phthalocyanines were rinsed with demineralized water and dried on filter paper. Samples were immersed in distilled water, maintaining a contact ratio of 1 dm^2/100 mL. Incubation was performed at 40 °C for 10 days (240 h) in the dark with mild agitation (110 rpm), representing standard migration conditions for long-term room temperature contact. Control samples (pure water and PVC without phthalocyanine) were prepared in parallel. The same prepared samples were also subjected to UV–Vis and EDX-XRF analysis, respectively.

Uv–vis analysis

Measurements were carried out on a Tecan Infinite 200 PRO (Tecan, Austria). Absorption spectra of the calibration series (0.01–5.0 μg/mL) were recorded in the range of 300–800 nm. The absorption maximum was determined at 628 nm, which was subsequently used for quantitative measurements. The limit of detection for this method was 0.24 μg of PTC per mL.

EDX-XRF analysis

The content of elements in the sample water extracts was determined by EDX-XRF method (Energy ray dispersion spectroscopy − X ray fluorescence), which is based on elemental analysis of X-ray diffraction (energy) materials. The amount of element analyzed was evaluated in weight percent (wt %).

Samples in special cups were placed (3 g) inside the instrument at the appropriate sample to autosampler. The content of the elements was determined using an Energy Dispersive X-ray Spectrometer (Thermo Scientific, ARL Quant X). The samples were analyzed in a special selected method: Any sample Air in Quant Unite program. The limit of

detection is until: 0.1 – 0.5 wt%, and the limit of quantification is until: 0,1 wt%.

Results and Discussion

Morphology analysis

The morphology of the prepared PVC samples was investigated by SEM. Representative surface micrographs of cryo-sectioned moulded foils are shown in Fig. 2. Discrete particulate features were observed within a narrow size range across all samples, including neat PVC (Fig. 2A), despite the absence of intentionally added additives. Their ubiquitous presence strongly suggests that these particulates originate from processing additives incorporated by the PVC granulate manufacturer to enhance material performance, as previously reported.[33,34] SEM images of the pure additives, provided in the Supplementary Material, support this interpretation, as the particles observed throughout the PVC samples, including the reference PVC, differ morphologically from both ZnPTC-HEMA and ZPT (Fig. S1).

In comparison with neat PVC (Fig. 2A), the PVC sample containing ZPT (0.005 wt%; Fig. 2G) exhibits a homogeneous morphology with no discernible ZPT particles, indicating good compatibility and dispersion of ZPT within the PVC matrix. Similarly, samples containing Zn-PTC-HEMA at lower loadings (Fig. 2B–E and Fig. 2H–K) display smooth fracture surfaces and a uniform distribution of PTC, with no evidence of particle agglomeration. Nevertheless, a gradual increase in the number of particulate features was observed with increasing ZnPTC-HEMA content, particularly from 0.5 wt% onward, suggesting concentration-dependent changes in the microstructure.

In contrast, samples containing 3 wt% Zn-PTC-HEMA, both without and with ZPT (Fig. 2F and Fig. 2L, respectively), show a homogeneous matrix populated by a markedly higher number of particulate features. Notably, sample L exhibits a significantly roughened fracture surface. This morphology is indicative of an excessive loading of the phthalocyanine additive, leading to microstructural heterogeneity. The observed surface roughness correlates well with the deterioration in mechanical properties discussed in the following section. Similar effects associated with high PTCs loadings in polymer matrices have been reported elsewhere.[22]

Chemical structure analysis by Fourier transform infrared spectroscopy (ATR-FTIR) and Nuclear Magnetic Resonance spectroscopy (NMR)

The FTIR spectrum of neat PVC exhibits characteristic absorption bands associated with specific functional groups in the repeating –CH_2–CHCl– units (Fig. 3). Strong bands at 2970–2850 cm^{-1} correspond to C–H stretching vibrations of the methylene (–CH_2–) groups, typical of aliphatic polymers and indicative of the saturated polymer backbone. The prominent band at 1425 cm^{-1} arises from CH_2 scissoring vibrations and is a key diagnostic feature of PVC. Additional bands in the 1330–1250 cm^{-1} region are assigned to CH_2 wagging and rocking modes, while those at 1095–1020 cm^{-1} correspond to C–C stretching vibrations along the polymer chain. A distinctive set of absorptions between 960 and 610 cm^{-1} is attributed to C–Cl stretching vibrations, which are characteristic of PVC and confirm the presence of chlorine in the macromolecular structure.

Bands near 1730 cm^{-1} (C=O stretching) and 1650 cm^{-1} (C=C stretching), which would indicate oxidation or dehydrochlorination, are absent, confirming that the material is chemically unaltered PVC. Overall, the obtained FTIR spectrum agrees well with reference data [36,37] and displays all diagnostic features of unmodified PVC, including pronounced C–H, CH_2, and C–Cl absorptions. The FTIR spectra of PVC formulations containing additives closely resemble that of neat PVC (PVC-0). In the ZPT-containing formulations, a weak but reproducible band appeared at approximately 1538 $cm^{-}1$, whereas this band was absent in neat PVC. This absorption is assigned to coordination-

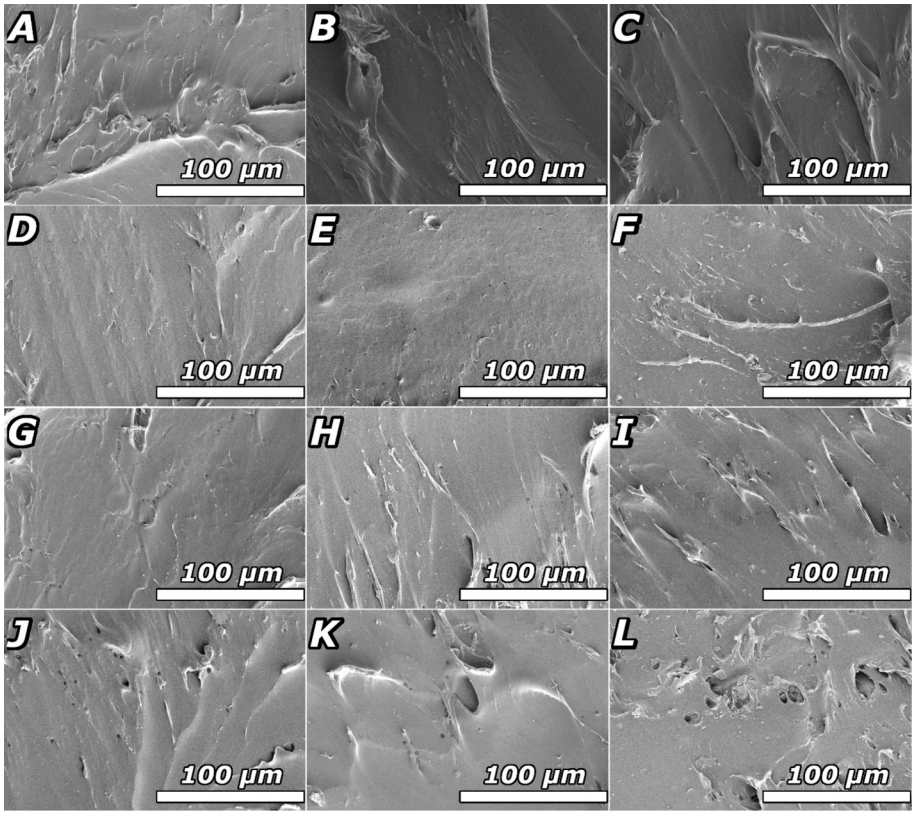


Fig. 2. SEM images of A) PVC-0, B) PVC-0.1, C) PVC-0.2, D) PVC-0.5, E) PVC-1, F) PVC-3, G) PVC-0-ZPT, H) PVC-0.1-ZPT, I) PVC-0.2-ZPT, J) PVC-0.5-ZPT, K) PVC-1-ZPT, L) PVC- 3-ZPT.

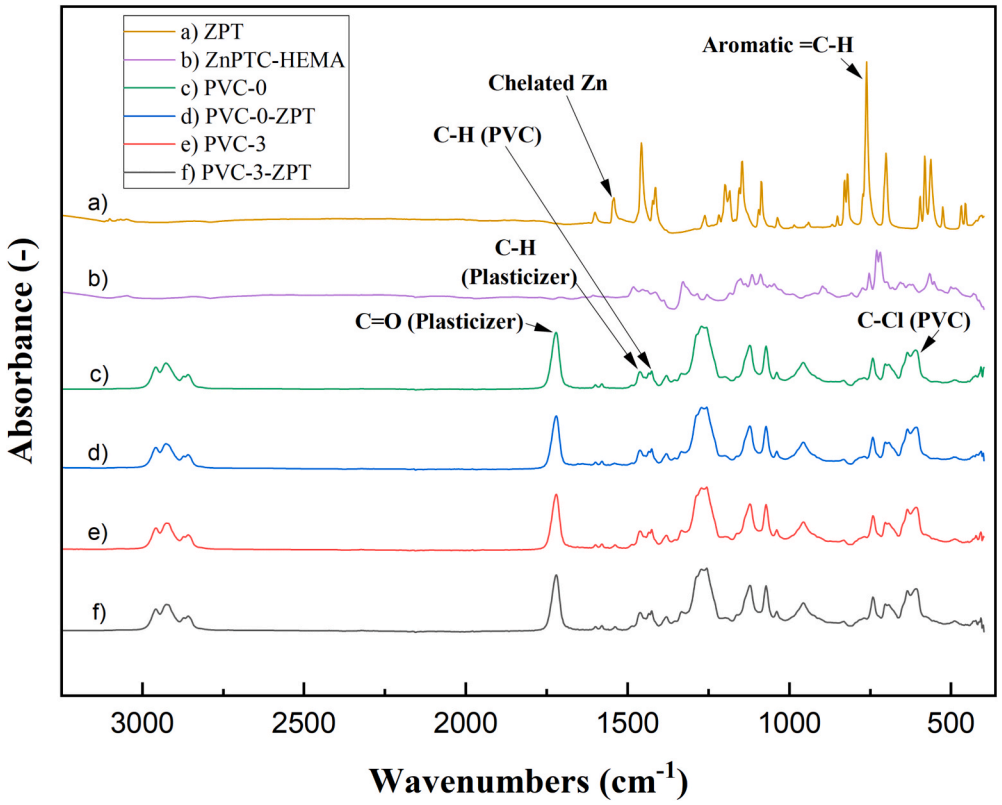


Fig. 3. FTIR spectra for pure ZnPTC-HEMA; a) pure ZPT, b) ZnPTC-HEMA, c) PVC-0, d) PVC-0-ZPT, e) PVC- 3 and f) PVC- 3-ZPT. In accordance with Deleanu et al. (2024).[35]

sensitive vibrations of the pyrithione ligand in the Zn–pyrithione complex. A similar band at approximately 1536 cm^{-1} has been reported for zinc pyrithione-containing polymer systems and was associated with oxygen coordination to Zn in a chelated form; in contrast, an ionic form would be expected to give a band closer to 1576 cm^{-1}.[38] Therefore, the presence of the ~ 1538 cm^{-1} band does not merely reflect the nominal addition of ZPT, but supports that the Zn–pyrithione coordination environment remained detectable after melt processing. The low intensity of this band is consistent with the very low ZPT loading used in this study (0.005 wt%) and with partial overlap with absorptions of the PVC matrix and formulation additives. Importantly, the characteristic PVC bands remained unchanged and no new bands attributable to oxidation, dehydrochlorination, or major chemical modification of the PVC matrix were observed.

FTIR spectroscopy shows that, even at the highest loadings of ZnPTC-HEMA and ZPT, the characteristic bands of PVC remain unchanged in position and relative intensity (Fig. 3). This indicates that incorporation of these additives does not alter the chemical environment of the PVC chains, implying the absence of chain rearrangement, disruption of the polymer backbone, or formation of new interactions that would modify the matrix structure.

To further support the successful incorporation of HEMA into the ZnPTC structure, ^{1}H and ^{13}C NMR spectra of ZnPTC-HEMA were recorded and compared with those of the ZnPTC-AA precursor (Fig. 4). Because non-symmetrically substituted phthalocyanines often provide complex NMR spectra due to regioisomerism, aggregation, π–π stacking, limited solubility, and the presence of multiple substitution patterns, complete peak-by-peak assignment is challenging.[39] Therefore, the interpretation was focused mainly on the most diagnostic differences between ZnPTC-AA and ZnPTC-HEMA. Since the phthalocyanine macrocycle is expected to be only negligibly affected by HEMA substitution, the newly appearing signals in ZnPTC-HEMA can be primarily attributed to the HEMA moiety bound to the previously introduced allyl group.

The most pronounced differences were observed in the ^{13}C NMR spectra (Fig. 4). In the aromatic/olefinic region, new resonances appeared at 166.7 ppm and 125.7 ppm, which were assigned to the ester carbonyl carbon and the methacrylate $=CH_2$ carbon, respectively. In the aliphatic region, additional signals at 66.1 and 58.9 ppm were attributed to the hydroxyethyl carbons of the HEMA substituent, while the signal at 18.0 ppm corresponded to the terminal methyl carbon of the methacrylate group. The presence of the HEMA substituent was further supported by ^{1}H NMR spectroscopy, which showed characteristic methacrylate vinyl proton signals at 6.05 and 5.69 ppm and a methacrylate methyl signal at 1.90 ppm. Together with the corresponding ^{13}C NMR resonances assigned to the ester carbonyl, olefinic carbon, oxygen-adjacent CH_2 carbons, and methyl carbon, these diagnostic signals were absent or not clearly detectable in the ZnPTC-AA precursor, supporting the successful incorporation of the HEMA moiety into the ZnPTC structure. This assignment is consistent with literature data for HEMA and methacrylate-containing derivatives, where methacrylate vinyl protons are typically observed at approximately 6.1 and 5.6 ppm, methacrylate methyl protons around 1.9 ppm, and the corresponding ^{13}C NMR signals near 167, 126, 60–66, and 18 ppm, respectively.[40,41] However, due to signal overlap and the complexity of the phthalocyanine spectra, the NMR data were used as qualitative evidence of HEMA incorporation rather than for quantitative determination of the substitution degree.

Colorimetric study

The transmission spectra (Fig. 5) of neat PVC (PVC-0) and PVC compounds containing ZnPTC-HEMA at different loadings (0.1–3.0 wt %), with and without the presence of ZPT (0.005 wt%), reveal distinct modifications in optical behavior that are strongly dependent on the concentration of ZnPTC-HEMA (Fig. 5).

Neat PVC exhibits a baseline spectrum typical of an unmodified

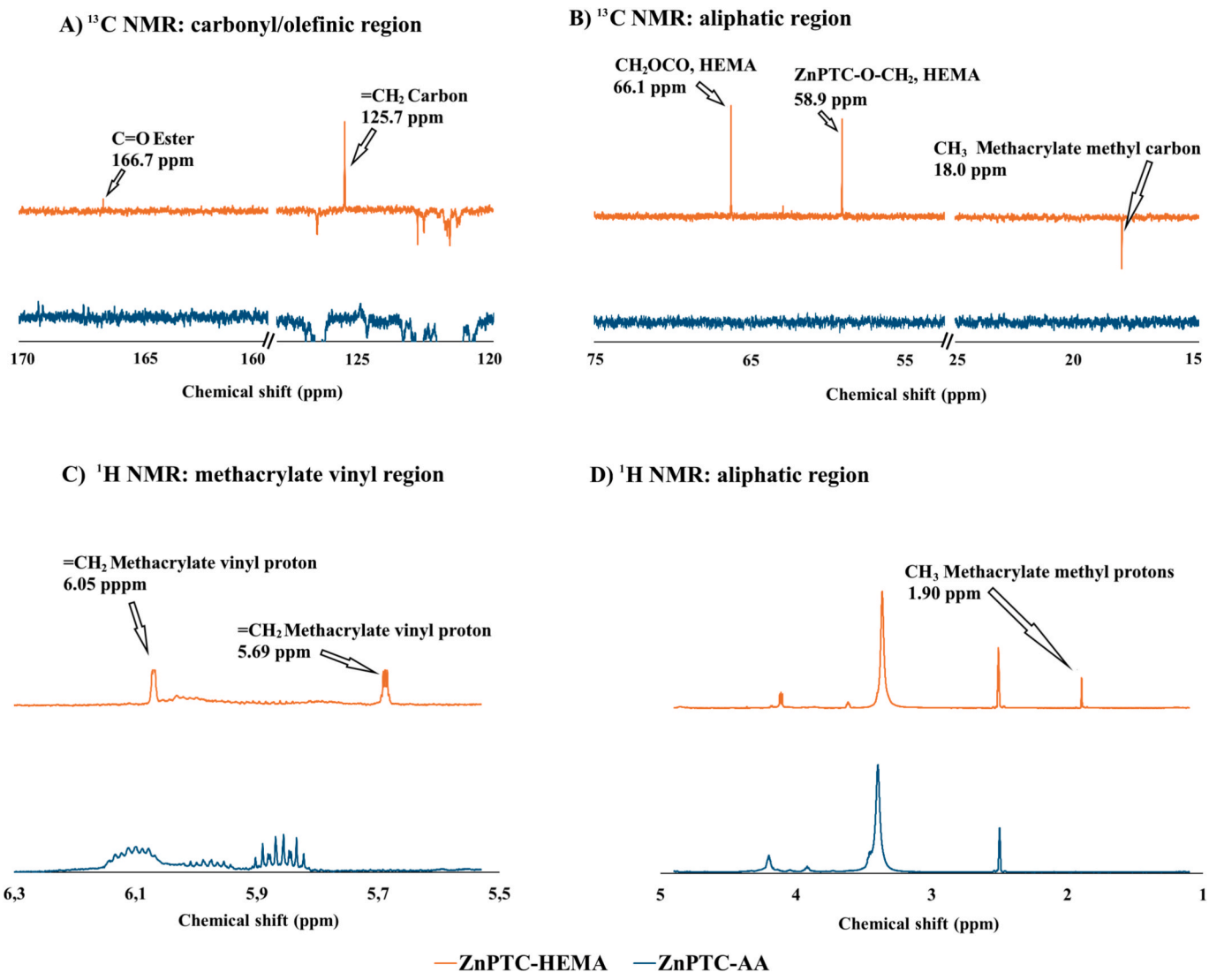


Fig. 4. Comparative NMR characterization of ZnPTC-AA and ZnPTC-HEMA.

polymer matrix, with relatively high transmission across the visible region and minimal absorption features.[42] Upon incorporation of ZnPTC-HEMA at low concentrations (0.1–0.2 wt%), a slight decrease in transmission is observed, indicating the introduction of weak absorptive species into the polymer matrix. The effect is slightly more pronounced with the simultaneous introduction of ZPT.

At concentrations of 0.5–1.0 wt% ZnPTC-HEMA, the spectra reveal a pronounced reduction in transmittance, most notably within the UV region. This trend is attributable to the increased absorbance associated with the higher density of ZnPTC-HEMA chromophore units. Co-addition of ZPT induces a further, albeit modest, decrease in transmittance; however, the relative influence of ZPT diminishes progressively with increasing ZnPTC-HEMA concentration.

At the highest concentration examined (3.0 wt% ZnPTC-HEMA; samples PVC-3 and PVC-3-ZPT), the spectra exhibit the lowest overall transmittance, characterized by substantial attenuation across both the UV and visible regions. Under these conditions, the presence of ZPT does not produce a significant additional suppression of transmittance, indicating that optical shielding is dominated by the ZnPTC-HEMA component at this concentration.

The visual appearance of the samples (Fig. 6) is fully consistent with the spectroscopic data. Increasing ZnPTC-HEMA concentration leads to a progressive darkening and loss of transparency, while samples with and without ZPT at the same ZnPTC-HEMA loading are visually indistinguishable or show only negligible differences. Together, these results demonstrate that the colorimetric and optical properties of the compounds are controlled almost exclusively by ZnPTC-HEMA content. The addition of ZPT at 0.005 wt% does not significantly affect the transmission behavior, confirming that ZPT can be incorporated without compromising the optical characteristics of the PVC/ZnPTC-HEMA compound.

Thermal properties

The applicability of antimicrobial agents incorporated into polymers is determined not only by their compatibility with the polymer matrix but also by their thermal stability. PVC undergoes thermal degradation in distinct stages. The initial degradation phase occurs between 25 °C and 350 °C and is primarily associated with dehydrochlorination and the volatilization of plasticizers, such as di(2-ethylhexyl) phthalate (DEHP).[43] This stage exhibited two distinct degradation events, with peak maxima at 255 °C and 280 °C. During this phase, a weight loss of approximately 72.4 wt% was observed, with the maximum degradation rate occurring at 280 °C (Table 2), as indicated by the peak temperature (Tp) on the DTG curve. This is in accordance with other studies of thermal behavior of PVC.[44,45]

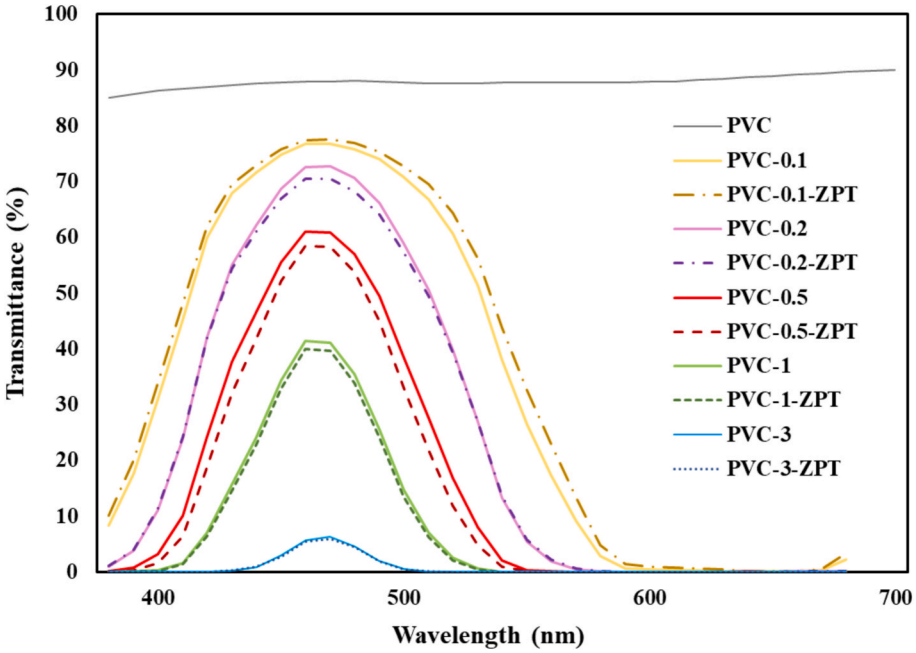


Fig. 5. Transmission spectra of PVC-0; PVC-0.1; PVC-0.1- ZPT; PVC-0.2; PVC-0.2-ZPT; PVC-0.5; PVC-0.5-ZPT; PVC-1; PVC-1-ZPT; PVC-3; PVC-3-ZPT.

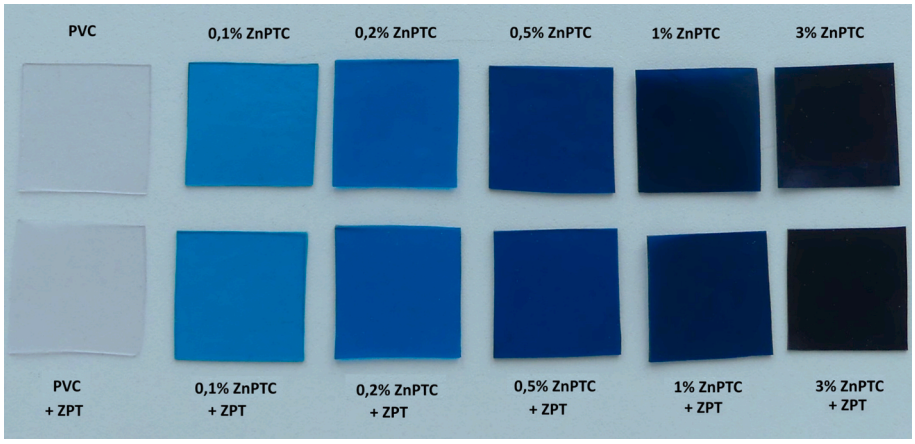


Fig. 6. PVC samples with increasing ZnPTC-HEMA; PVC-0, PVC-0.1, PVC-0.2, PVC-0.5, PVC-1, PVC-3; (top) and with the addition of ZPT (0.005 wt%); PVC-0.1-ZPT, PVC-0.2-ZPT, PVC-0.5-ZPT, PVC-1-ZPT, PVC- 3-ZPT (bottom).

Table 2
Thermal characterization analysis of antimicrobial additives and PVC.

Samples	T_i (°C)	T_p (°C)	Temperature range (°C) Weight loss (wt %)		
			25–350	**350–600**	**600–800**
PVC-0	197	280	72.38	19.23	0.80
PVC- 3-ZPT	200	278	71.11	15.81	1.49
			25–150	**150–420**	**420–800**
ZnPTC-HEMA		322	3.70	23.07	37.2
			25–420	**420–600**	**600–800**
ZPT	265	282	49.04	5.53	5.31

The initial decomposition (onset) temperature (T_i), the peak maximum on DTG curve T_p

The second degradation stage occurred between 350 °C and 600 °C and is likely associated with the breakdown of conjugated polyenes into benzene and alkylated benzenes, as well as the thermal cracking of the polymer backbone. Finally, at temperatures above 600 °C, the last degradation stage takes place, which can be attributed to the decomposition of byproducts, such as hydrocarbon residues, formed during the earlier degradation processes.[45–47]

The incorporation of the antimicrobial agents ZPT and ZnPTC-HEMA had only a minor effect on the thermal degradation behavior of PVC. Unlike neat PVC (PVC-0), the compound material (PVC-3-ZPT) exhibited a single broad degradation step in the temperature range of 25 °C to 350 °C, with a peak maximum at 280 °C, which is characteristic of PVC with no significant difference in weight loss. The influence of the antimicrobial agents became more apparent in the subsequent degradation stages. Although these stages occurred within the same temperature ranges as for neat PVC, they exhibited varying weight changes. Specifically, the second degradation step showed reduced weight loss in the presence of ZPT, while the addition of ZnPTC-HEMA resulted in increased weight loss during the final degradation stage. To support these observations, TGA of the pure antimicrobial agents was also conducted to better understand their individual thermal degradation behaviors. Overall, the total weight loss was approximately 92.41 wt% for neat PVC (PVC-0) and 88.41 wt% for the PVC/ZPT/ZnPTC-HEMA compound (PVC-3-ZPT).

For the pure ZPT, the degradation initiation temperature was

observed at approximately 265 °C, with the first peak maximum occurring at 282 °C (Table 2). The overall thermal decomposition can be divided into three distinct degradation stages. The first stage, associated with the decomposition of the ZPT complex, occurred within the temperature range of 25 °C to 420 °C. This stage exhibited two distinct degradation events, with peak maxima at 282 °C and 330 °C, which are consistent with values reported in the literature.[48] These peaks are attributed to the solid-state dimeric structure of ZPT.

The second degradation stage, characterized by a weight loss of 5.53 wt%, occurred between 420 °C and 600 °C and is likely associated with the degradation of specific components of the ZPT complex. The final degradation stage, observed at temperatures above 600 °C, is attributed to the decomposition of residual byproducts.

Additionally, ZPT exhibits a melting point of approximately 240 °C, which facilitates its incorporation into a range of thermoplastics and elastomers. Notably, previous studies have shown that the addition of ZPT does not compromise the thermal stability of high-density polyethylene (HDPE) foils, indicating that ZPT can be effectively used in polymer matrices without significantly affecting their thermal properties.[49]

The thermal stability of the pure ZnPTC-HEMA dye was also evaluated using the TGA. The TGA curve revealed multiple decomposition steps. The initial weight loss of 3.70 wt% was observed from room temperature up to 150 °C (Table 2), corresponding to the evaporation of adsorbed moisture.

The degradation behavior of this newly synthesized material was complex and analyzed in terms of the decomposition of its constituent components. Specifically, the PTC segment degraded in two distinct temperature intervals, with degradation of the HEMA component occurring between these stages. The soft HEMA segments degraded in the temperature range of 200 °C to 420 °C, with a maximum degradation rate at 322 °C. Additionally, the initial degradation of the PTC component began earlier, between 150 °C and 200 °C, and was attributed to the breakdown of the phthalocyanine ring.

At elevated temperatures above 420 °C, the degradation of both the PTC component and the hard HEMA segments continued, with overlapping processes that prevented the clear distinction of individual degradation steps. For instance, the hard HEMA segments were expected to degrade within the range of 327 °C to 670 °C, while the residual PTC component decomposed between 450 °C and 700 °C. Despite the complexity, the overall decomposition behavior observed in this study is consistent with previously reported findings.[50–52]

DSC measurements were also performed to evaluate possible thermal transitions of the PVC-based formulations. However, due to the highly plasticized and low-crystallinity/amorphous character of the investigated medical-grade PVC compound, the thermograms did not show well-resolved melting or crystallization transitions suitable for reliable comparative analysis. The weak and broad thermal features were strongly influenced by the plasticized matrix and sample thermal history. Therefore, DSC did not provide additional conclusive information on the effect of ZnPTC-HEMA or ZPT incorporation, and the thermal evaluation was based primarily on TGA/DTG, which more directly reflects the stability of the additives and PVC compound under melt-processing conditions.

Mechanical properties

The mechanical properties of neat PVC (PVC-0) and PVC compounds containing 0.1 and 3 wt% ZnPTC-HEMA, prepared with and without ZPT, are summarized in Table 3. The Young's modulus of PVC-0 (10.2 ± 0.8 MPa) is not affected by the incorporation of a low loading of ZnPTC-HEMA (0.1 wt%) nor by the presence of ZPT. In contrast, increasing the ZnPTC-HEMA content to 3 wt% (PVC-3) leads to a measurable stiffening of the material, with the modulus rising to 12.6 ± 1.7 MPa in the absence of ZPT and to 13.0 ± 1.9 MPa when ZPT is present (PVC-3-ZPT). Statistical analysis using a two-sample Student's t-test ($\alpha = 0.05$, 95 % confidence level), performed relative to neat PVC, confirms that this increase is statistically significant only at the highest phthalocyanine loading (3 wt%), irrespective of ZPT addition. This trend is consistent with the morphological features observed in the SEM micrographs, which indicate a more rigid microstructure at higher additive contents.

Table 3
Mechanical Properties of PVC and ZnPTC-HEMA Compounds with/without ZPT (0.005 wt%).

Samples	Young Modulus (MPa)	Strain at Break (%)	Stress at Break (MPa)
PVC-0	10.2 ± 0.8^{a}	185.5 ± 35.0^{a}	9.7 ± 1.9^{a}
PVC-0.1	10.8 ± 0.6^{a}	174.4 ± 34.8^{a}	8.0 ± 1.4^{a}
PVC- 3	12.6 ± 1.7^{b}	196.6 ± 26.2^{a}	9.9 ± 1.8^{a}
PVC-0-ZPT	9.7 ± 0.7^{a}	172.5 ± 22.4^{a}	9.2 ± 1.8^{a}
PVC-0.1-ZPT	10.8 ± 0.1^{a}	196.5 ± 35.7^{a}	7.5 ± 1.4^{a}
PVC-3-ZPT	13.0 ± 1.9^{b}	186.3 ± 36.3^{a}	9.7 ± 1.9^{a}

The tensile strength (stress at break) of all samples falls within a narrow range of 7.5 ± 1.4 to 9.9 ± 1.8 MPa, while the strain at break varies between 174.4 ± 34.8 % and 196.6 ± 26.2 % (Table 3). No statistically significant differences in either tensile strength or elongation at break are observed compared to neat PVC (PVC-0). These results indicate that, within the investigated concentration range, ZnPTC-HEMA does not detrimentally affect the ductility or ultimate strength of the PVC matrix.

Pronounced effects of phthalocyanines on polymer mechanical properties have been reported previously, for example for copper phthalocyanine incorporated into a polyurethane matrix; however, such effects were observed at substantially higher filler loadings (up to 30 wt %) (Youssef, Al-Turaif, and Wazzan 2015). In contrast, our findings are in line with reports describing negligible changes in mechanical performance upon the incorporation of moderate amounts of photocatalytic additives into PVC, such as 4.8 wt% reported by Yang et al. (2016). Overall, the present results demonstrate that low to moderate ZnPTC-HEMA loadings preserve the mechanical integrity of PVC, while higher loadings can induce a modest but statistically significant increase in stiffness without compromising tensile strength or elongation.

Singlet oxygen quantification

The quantitative analysis of singlet oxygen generation, summarized in the Table 3, demonstrates that incorporation of ZnPTC-HEMA into the PVC matrix markedly enhances singlet oxygen production relative to neat PVC. The pristine polymer exhibits a very low rate constant ($k = 0.0031\ J^{-1}$) and a correspondingly long half-time ($\tau_1/_2 \approx 5590$ s), confirming the negligible intrinsic photosensitizing activity of unmodified PVC under the applied experimental conditions.

Even at the lowest ZnPTC-HEMA loading of 0.1 wt% (PVC-0.1), a pronounced increase in singlet oxygen generation is observed, with k increasing by nearly an order of magnitude and $\tau_1/_2$ decreasing to approximately 600 s. This sharp transition indicates that ZnPTC-HEMA acts as a highly efficient photosensitizer within the polymer matrix and that only minimal additive concentrations are required to activate effective photodynamic behavior. As the ZnPTC-HEMA content increases from 0.1 to 1 wt% (PVC-1 to PVC-1), a monotonic increase in k is accompanied by a progressive reduction in $\tau_1/_2$, reflecting accelerated singlet oxygen production. The most substantial gains occur up to approximately 0.5–1 wt% (PVC-0.5 to PVC-1), beyond which further increases in additive content yield only marginal improvements.

At higher loadings (1–3 wt%), the system approaches a plateau regime, with k values converging to $\sim 0.05\ J^{-1}$ and $\tau_1/_2$ stabilizing in the range of 317–333 s. This saturation behavior suggests that singlet oxygen generation becomes limited by factors other than photosensitizer concentration, such as light absorption efficiency, excited-state

quenching, or oxygen diffusion within the polymer matrix.

The addition of ZPT at 0.005 wt% (Table 4) leads to a modest reduction in singlet oxygen generation across all ZnPTC-HEMA concentrations. This effect is reflected in slightly lower k values and correspondingly higher $\tau_1/_2$ values relative to the ZPT-free systems. Importantly, the preservation of high singlet oxygen production in the presence of ZPT indicates that the two antimicrobial strategies, single oxygen production and conventional biocidal action, can coexist without strong antagonistic interactions. This observation is consistent with the antimicrobial assay results, which show sustained efficacy even in formulations containing both additives. From an application perspective, these findings support the feasibility of designing multifunctional PVC materials in which ZnPTC-HEMA provides robust photodynamic activity at relatively low loadings, while ZPT contributes complementary antimicrobial protection without significantly impairing ROS generation.

All samples were analyzed in triplicate. The relative standard deviation (RSD) for replicate measurements was below 10 % for each sample, demonstrating good repeatability of the analytical procedure. Accordingly, the measured values were deemed sufficiently reliable for subsequent evaluation of photoactivity.

Overall, the singlet oxygen quantification data highlight an optimal ZnPTC-HEMA concentration window around 0.5–1 wt%, where high photodynamic efficiency is achieved without unnecessary additive excess. This balance is particularly relevant for practical implementation, as it aligns enhanced antimicrobial performance with material stability and processability requirements expected for advanced polymeric antimicrobial surfaces.

Antimicrobial assays

Antibacterial efficacy

The study results demonstrated that PVC modified with phthalocyanine derivate ZnPTC-HEMA exhibits pronounced light-activated antimicrobial activity. Under illumination at 1000 lx, the material effectively suppressed the growth of Gram-positive *S. aureus* even at a loading of 0.1 % (PVC-0.1), indicating a bactericidal response (Fig. 7). In contrast, Gram-negative *E. coli* showed substantially lower susceptibility: only weak inhibition was observed at ZnPTC-HEMA concentrations up to 0.5 % ($R = 1.4 \pm 0.2$), while strong antimicrobial activity ($R = 3.8 \pm 0.1$) was achieved only at the highest loading tested (3 %) under light exposure. Samples incubated in the dark exhibited only marginal activity ($R = 1.6 \pm 0.2$), detectable solely against *S. aureus* at loadings ≥ 1 %, indicating that the effect is primarily photoactivation-driven rather than due to passive toxicity of the material.

The addition of ZPT (0.005 wt%) significantly ($P > 0.05$) enhanced the antimicrobial properties, even in non-illuminated samples (Fig. 8). The figure shows that antimicrobial efficiency depends on the dye concentration. This enhancement was notable, as strong antimicrobial activity ($R > 3$) against both monitored bacteria strains at only 0.5 % ZnPTC-HEMA (PVC-0.5-ZPT), suggesting a synergistic enhancement of photodynamic activity.

Table 4
Singlet oxygen production as a function of ZnPTC-HEMA concentration with/without fixed ZPT loading (0.005 wt%).

Sample	ZnPTC-HEMA (wt %)	ZPT (wt %)	k (J^{-1})	$\tau_{1/2}$ (s)
PVC-0	–	–	0.0031	5590
PVC-0.1	0.1	–	0.0287	604
PVC-0.2	0.2	–	0.0373	465
PVC-0.5	0.5	–	0.0492	352
PVC-1	1.0	–	0.0521	333
PVC-3	3.0	–	0.0547	317
PVC-0.1-ZPT	0.1	0.005	0.0272	637
PVC-0.2-ZPT	0.2	0.005	0.0368	471
PVC-0.5-ZPT	0.5	0.005	0.0463	374
PVC-1-ZPT	1.0	0.005	0.0502	345
PVC-3-ZPT	3.0	0.005	0.0452	383

All samples were analyzed in triplicate. The relative standard deviation (RSD) for replicate measurements was below 10 % for each sample.

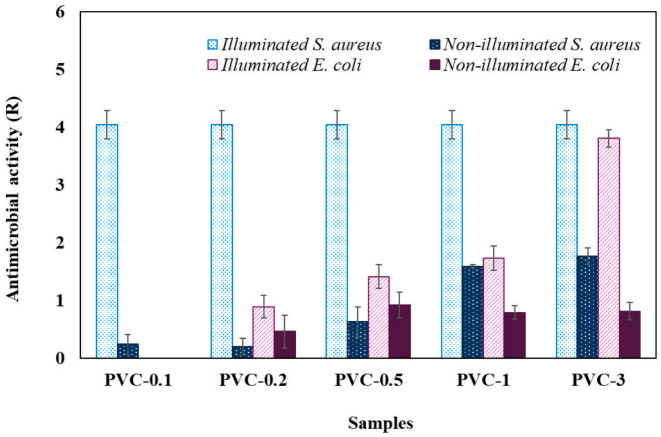


Fig. 7. Antibacterial activity of illuminated/non-illuminated PVC samples with ZnPTC-HEMA concentration scale against *S. aureus* and *E. coli.*

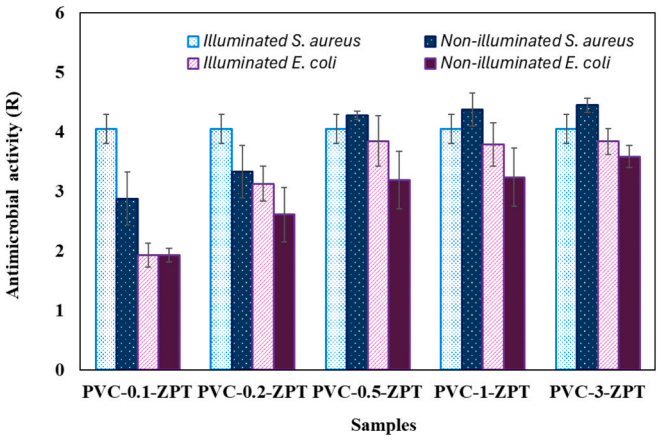


Fig. 8. Antibacterial activity of of illuminated/non-illuminated PVC samples with ZnPTC-HEMA concentration scale and ZPT (0.005 wt%) against *S. aureus* and *E. coli.*

The results of the antibacterial activity assessment, summarized in Figs. 6 and 7, reveal higher efficacy against Gram-positive *S. aureus*. This observation aligns with findings reported in previous studies.[18,22] Grammatikova et al. (2019) demonstrated a strong antibacterial effect of phthalocyanine-stained paper against *S. aureus* after just 60 min of exposure to light at an intensity of 270 lx.[14] Similarly, Mapukata et al. (2021) also reported high antibacterial activity against *S. aureus* under illumination.[53]

The photodynamic mechanism of phthalocyanines is well established and involves light absorption followed by intersystem crossing to the triplet excited state and subsequent electron energy transfer to molecular oxygen. This process generates reactive oxygen species, including singlet oxygen, which exhibit potent antibacterial effects.[53] Some studies have shown that these species can penetrate the porous peptidoglycan layer of Gram-positive bacteria, making them more susceptible to photodynamic inactivation.[54–56]

In contrast, Gram-negative bacteria possess an additional outer lipopolysaccharide layer, which reduces their permeability to lipophilic small molecules and increases their resistance to both antibiotics and photodynamic treatments. However, the photosensitivity of Gram-negative bacteria can be enhanced by substances such as $CaCl_2$, EDTA, or polymyxin B, which alter outer membrane permeability. The

underlying reasons for Gram-negative bacteria's resistance to photosensitization remain unclear but may involve the charge on the photosensitizer and its resulting subcellular distribution and localization within these organisms.[54,55] Additionally, weak antimicrobial activity against *E. coli* was also recently demonstrated for a polyhydroxybutyrate submicron fibber mat with 0.1 wt% zinc phthalocyanine derivative content.[56]

To further support the interpretation of the antimicrobial mechanism, additional MIC experiments were performed for the individual antimicrobial additives ZnPTC-HEMA and ZPT. Since MIC determination is not directly applicable to the final PVC specimens, which are solid polymeric surfaces, the test was conducted using the free antimicrobial additives. The detailed methodology and results are provided in the Supplementary Material, Table S1. Briefly, ZnPTC-HEMA showed light-dependent antibacterial activity, with an MIC of 2 mg/L and a bactericidal concentration of 16 mg/L against *S. aureus* under illumination, whereas the MIC in the dark exceeded the tested concentration range (>64 mg/L). Against *E. coli*, illuminated ZnPTC-HEMA showed an MIC of 16 mg/L, while the bactericidal concentration exceeded the tested concentration range. ZPT exhibited antibacterial activity, with MIC values of 4 mg/L for *S. aureus* and 2 mg/L for *E. coli*.

Antiviral efficacy

The antiviral activity of the prepared samples was assessed following the ISO 22196:2021 standard, with protocol modifications to accommodate bacteriophage propagation requirements. Table 5 summarizes the antiviral performance of illuminated and non-illuminated PVC specimens incorporating increasing concentrations of ZnPTC-HEMA. Antiviral efficacy was assessed against the enveloped bacteriophage Φ6 and the non-enveloped bacteriophage ΦX174.

The results demonstrate that incorporation of 0.1 wt% ZnPTC-HEMA yields (PVC-0.1) a statistically significant ($P < 0.05$) microbicidal effect against Φ6 under light irradiation ($R = 5.1 \pm 0.2$). In contrast, no measurable antiviral activity was detected in samples maintained under dark conditions. Furthermore, no reduction in infectivity was observed for ΦX174 under either illuminated or non-illuminated conditions, indicating that singlet oxygen generated upon irradiation selectively inactivates the enveloped bacteriophage Φ6 but does not affect the non-enveloped ΦX174.

The antiviral test results in Table 6 indicate, in contrast to the tested bacteria, that the addition of ZPT did not improve the antiviral efficacy of the samples against either tested bacteriophage.

The pronounced antiviral efficacy of singlet oxygen against bacteriophage Φ6 was expected, as its effectiveness against enveloped viruses has been documented in several studies.[57,58] Efimov et al. (2024) reported a 99.97 % (3.4 log) reduction in the viral load of enveloped SARS-CoV 227 upon light exposure of fabrics functionalized with the tetracationic zinc phthalocyanine derivative LASU.[15]

Singlet oxygen is highly active and readily reacts with diverse biological macromolecules, including nucleic acids, proteins, and lipids. In DNA, it preferentially oxidizes guanine residues and can induce covalent cross-links between guanine and lysine.[29] In enveloped viruses, singlet oxygen also targets the lipid components of the viral envelope, a phospholipid bilayer embedded with membrane proteins and receptor-binding glycoproteins, leading to oxidative damage that compromises viral integrity and infectivity.[57,59]

Pyrithione has been shown to inhibit infection by human rhinovirus, coxsackievirus, and mengovirus, RNA viruses belonging to the *Picornaviridae* family. Additionally, Qiu et al. (2013) reported that pyrithione exhibits inhibitory activity against HSV-1 and HSV-2 at non-cytotoxic concentrations. These viruses, members of the *Herpesviridae* family, are large DNA viruses.[60] Although phage Φ6, a member of the *Cystoviridae* family, has been successfully used as a surrogate for enveloped viruses, incorporation of 50 mg of ZPT to PVC did not produce measurable antiviral activity. This concentration was selected in accordance with the manufacturer's recommendation (Alchimica CZ), but it appears to be insufficient to elicit an antiviral effect under the conditions tested. Moreover, in contrast to the bacterial assays, no synergistic interaction was observed. Increasing the zinc pyrithione content to 0.01 wt% likewise failed to enhance antiviral efficacy.

Phage ΦX174 is one of the most resilient non-enveloped viruses, with an outer wall composed of a robust protein coat that withstands most disinfectants.[61] Our findings show that it resisted even the highest tested concentration of ZnPTC-HEMA in the PVC matrix at 3 wt% and the addition of ZPT (0.005 wt%).

Application relevance of the photoactivated antimicrobial effect

The antimicrobial performance observed in this study is primarily relevant to illuminated, oxygen-accessible surfaces, where the ZnPTC-HEMA photosensitizer can be activated by visible or ambient artificial light and generate reactive oxygen species.[14,15] Therefore, the developed material should be considered mainly for non-implantable and externally exposed PVC-based components rather than for permanently occluded or dark environments. Suitable application scenarios include high-touch healthcare surfaces, external parts of medical devices, protective films, polymer covers, handles, touch panels, bed-contact or wall-contact surfaces, and other semi-transparent or opaque PVC-based components exposed to indoor lighting. Such surfaces are relevant because high-touch areas in healthcare facilities are frequently contacted by patients and healthcare workers and are recognized as important targets for cleaning, disinfection, and antimicrobial surface strategies.[62] Importantly, the photoactivated material should be regarded as a complementary surface-disinfection approach rather than a replacement for standard hygiene procedures. The presence of ZPT provides additional antibacterial activity under dark conditions; however, the antiviral effect remained mainly light-dependent in the present study. Therefore, practical implementation should prioritize applications with regular exposure to ambient or artificial light and should further consider durability under cleaning, abrasion, and long-term illumination conditions.

Migration study evaluation

The objective of this study was to assess whether ZnPTC-HEMA migrates from PVC into an aqueous environment and, if so, to quantify its concentration. After 10 days of exposure (40 °C, distilled water), ZnPTC-HEMA was not detected in any of the eluates (c < LOD) by UV–Vis analysis and EDX method. These findings suggest strong retention of

Table 5
Antiviral activity of illuminated/non-illuminated PVC samples with ZnPTC-HEMA concentration scale.

Sample → **Phage ↓**	**ZnPTC-HEMA (wt %) →**	**PVC-0.1** **0.1**	**PVC-0.2** **0.2**	**PVC-1** **1**	**PVC-3** **3**
R Φ6	Illuminated	5.1 ± 0.2	5.1 ± 0.2	5.1 ± 0.2	5.1 ± 0.2
	Non-illuminated	0 ± 0.0	0.1 ± 0.0	0 ± 0.0	0 ± 0.0
R ΦX174	Illuminated	–	–	–	0.2 ± 0.02
	Non-illuminated	–	–	–	0 ± 0.0

Table 6
Antiviral activity of illuminated/non-illuminated PVC samples with ZnPTC-HEMA concentration scale and ZPT (0.005 wt%).

Sample → Phage ↓	ZnPTC-HEMA (wt %) →	PVC-0.1-ZPT 0.1	PVC-0.2-ZPT 0.2	PVC-1-ZPT 1	PVC-3-ZPT 3
R Φ6	Illuminated	5.2 ± 0.2	5.2 ± 0.2	5.2 ± 0.2	5.2 ± 0.2
	Non-illuminated	0 ± 0.0	0.1 ± 0.0	0 ± 0.0	0 ± 0.0
R ΦX174	Illuminated	–	–	–	0.5 ± 0.1
	Non-illuminated	–	–	–	0.4 ± 0.1

ZnPTC-HEMA within the PVC matrix, likely attributable to its high molecular weight and low aqueous solubility.

Limitations and future directions

Despite the promising performance demonstrated herein, several limitations should be acknowledged. Antiviral efficacy was evaluated using bacteriophage surrogates under controlled laboratory conditions; although Φ6 and ΦX174 are well-established models for enveloped and non-enveloped viruses, respectively; validation against clinically relevant human viruses will be required to fully determine the translational relevance of this material platform.

Another practical limitation is related to the optical properties of the modified PVC. Incorporation of ZnPTC-HEMA, particularly at loadings above 0.5 wt%, reduces the transparency of the PVC matrix due to the strong visible-light absorption of the phthalocyanine chromophore. Consequently, this material system is not primarily suitable for medical products where high optical clarity is essential, such as blood bags, transparent tubing, or devices requiring direct visual monitoring of fluids. Low ZnPTC-HEMA loadings, especially 0.1–0.2 wt%, appear to offer the most practical balance, as they retain a more acceptable optical appearance while already providing strong photoactivated antiviral activity against Φ6 and antibacterial activity against *S. aureus*.

Since the antimicrobial mechanism of ZnPTC-HEMA is primarily photoactivated, practical use should focus on surfaces that are regularly exposed to indoor daylight or artificial visible light and have access to molecular oxygen. Permanently dark, occluded, implanted, or intravascular applications are therefore not the primary target of this material platform unless an appropriate illumination strategy and full biological safety validation are provided. The addition of ZPT can partially complement this limitation by providing dark-active antibacterial activity; however, the antiviral effect observed in this study remained mainly light-dependent.

In addition, long-term photostability, durability under repeated cleaning or mechanical abrasion, and performance in complex biological matrices were not assessed. Future work should therefore address real-world aging behavior, biofilm formation under continuous use, cytocompatibility and regulatory safety considerations, and optimization of photosensitizer architecture to enhance activity against Gram-negative bacteria and non-enveloped viruses. Such investigations will be essential for advancing this platform toward practical medical and high-touch surface applications.

Conclusion

This study shows that incorporation of a methacrylate-functionalized zinc phthalocyanine (ZnPTC-HEMA) into PVC provides efficient, light-activated antimicrobial functionality at remarkably low additive loadings. Singlet oxygen generation increased sharply at 0.1 wt% and approached a plateau above approximately 1 wt%, identifying a practical composition window that balances photoactivity, processability, of material properties. Under visible light, the materials achieved complete photoinactivation (>5 log reduction) of the enveloped bacteriophage Φ6, while the structurally robust non-enveloped ΦX174 remained unaffected, underscoring the key role of lipid envelope oxidation in the antiviral mechanism.

The materials also exhibited pronounced photodynamic antibacterial activity, particularly against *S. aureus*, while *E. coli* required higher photosensitizer loadings, consistent with the grater permeability barrier of Gram-negative cell envelopes. Incorporation of ZPT at 0.005 wt% provided complementary dark-active antibacterial protection and broadened the antimicrobial profile without substantially reducing reactive oxygen species generation.

Materials characterization further confirmed good compatibility of the antimicrobial additives with the PVC matrix across the practically relevant concentration range. Noticeable structural disruption was observed only at the highest loading tested (3 wt% ZnPTC-HEMA), in agreement with the mechanical data. Statistically significant deterioration in mechanical performance was likewise detected only at this concentration, indicating that lower additive contents preserve the structural and functional integrity of the PVC foils. FTIR analysis showed that even the highest concentrations of ZnPTC-HEMA and ZPT did not measurably alter the chemical environment of the PVC chains. In addition, migration experiments revealed negligible additive release, supporting the stability of the material system during prolonged aqueous exposure.

Overall, the combination of strong photodynamic antiviral activity against an enveloped virus surrogate, enhanced antibacterial performance, retained mechanical integrity at low additive loadings, and minimal additive migration establishes ZnPTC-HEMA-modified PVC as a promising platform for antimicrobial polymer surfaces. From an application perspective, this material system appears most suitable for illuminated, oxygen-accessible, opaque or semi-transparent PVC-based high-touch surfaces and external medical-device components, where antimicrobial functionality is prioritized over full optical clarity. More broadly, these findings demonstrate the feasibility of integrating photoactive phthalocyanines into melt-processable PVC formulations to produce multifunctional materials for complementary passive and light-triggered surface disinfection.

CRediT authorship contribution statement

Hana Pistekova: Writing – original draft, Visualization, Validation, Methodology, Investigation, Formal analysis, Data curation, Conceptualization. **Martina Pummerova:** Writing – review & editing, Validation, Methodology, Investigation, Data curation. **Monika Strasakova:** Formal analysis. **Miroslava Dusankova:** Formal analysis. **Martin Novak:** Formal analysis. **Radka Korinková:** Formal analysis. **Vojtech Trousil:** Formal analysis. **Dominika Hanusova:** Formal analysis. **Jakub Sevcik:** Formal analysis. **Eva Domincova Bergerova:** Formal analysis. **Vladimir Sedlarik:** Validation, Supervision.

Declaration of competing interest

The authors declare that they have no known competing financial interests or personal relationships that could have appeared to influence the work reported in this paper.

Acknowledgments

This work was supported from the European Just Transition Fund within the Operational Programme: Just Transition under the aegis of the Ministry of the Environment of the Czech Republic, project Operational Programme Johannes Amos Comenius OP JAC "Application potential development in the field of polymer materials in the context of circular economy compliance (POCEK)", number CZ.02.01.01/00/23_021/0009004.

Authors are further grateful for co-funding from the development process of Centre of Polymer Systems, Tomas Bata University in Zlin, program DKRVO (RP/CPS/2024-28/002) supported by the Ministry of Education Youth and Sports of the Czech Republic.

This work was also co-financed with the state support of the Technology Agency of the Czech Republic within the TREND Programme, number FW03010006, "Permanent protection of touch screens to prevent the deposition of organic pollutants on their surface."

Appendix A. Supplementary data

Supplementary data to this article can be found online at https://doi.org/10.1016/j.jiec.2026.06.020.

References

[1] J. Dunning, R.S. Thwaites, P.J.M. Openshaw, Mucosal Immunol. 13 (4) (2020) 566–573, https://doi.org/10.1038/s41385-020-0287-5.
[2] W.N. Harrington, C.M. Kackos, R.J. Webby, Exp. Mol. Med. 53 (5) (2021) 737–749, https://doi.org/10.1038/s12276-021-00603-0.
[3] M. Ordon,, P. Nawrotek,, X. Stachurska,, M. Mizielińska, Coatings 2021 11(10) (2021) 1179. 10.3390/COATINGS11101179.
[4] D.M. Morens, J.K. Taubenberger, A.S. Fauci, J Infect Dis 198 (7) (2008) 962–970, https://doi.org/10.1086/591708.
[5] E. Olewnik-Kruszkowska, M. Gierszewska, E. Jakubowska, I. Tarach, V. Sedlarik, M. Pummerova, Polymers (basel). 11 (12) (2019) 2093, https://doi.org/10.3390/polym11122093.
[6] A. Donnadio, L. Roscini, A. Di Michele, V. Corazzini, G. Cardinali, V. Ambrogi, Mater. Sci. Eng. C 128 (2021) 112290, https://doi.org/10.1016/j.msec.2021.112290.
[7] A. Elgharbawy, Journal of Risk Analysis and Crisis Response 12(3) (2022). 10.54560/jracr.v12i3.335.
[8] S.T. Rabie, R.A. Abdel-Monem, O.M. Darwesh, S.T. Gaballah, Polym. Bull. 80 (8) (2023) 8899–8918, https://doi.org/10.1007/s00289-022-04478-7.
[9] S.T. Gaballah, A.M. Khalil, S.T. Rabie, J. Vinyl Add. Tech. 25 (2019) S1, https://doi.org/10.1002/vnl.21670.
[10] S. Rabie,, D. Ali,, N. Khaireldin,, M. El-Hashash,, M. Elsaidi,, A. El-Sayed,, N. Wahed, Egypt. J. Chem. 0(0) (2020) 0–0. 10.21608/ejchem.2020.28830.2618.
[11] A.M. Khalil, S.T. Rabie, J. Vinyl Add. Tech. 23 (2017) S1, https://doi.org/10.1002/vnl.21588.
[12] S.T. Gaballah, H.A. El-Nazer, R.A. Abdel-Monem, M.A. El-Liethy, B.A. Hemdan, S. T. Rabie, Int. J. Biol. Macromol. 121 (2019) 707–717, https://doi.org/10.1016/j.ijbiomac.2018.10.085.
[13] R.A. Abdel-Monem, S.T. Gaballah, S.T. Rabie, J. Vinyl Add. Tech. 30 (2) (2024) 439–455, https://doi.org/10.1002/vnl.22059.
[14] N.E. Grammatikova, L. George, Z. Ahmed, N.R. Candeias, N.A. Durandin, A. Efimov, J. Mater. Chem. B 7 (28) (2019) 4379–4384, https://doi.org/10.1039/C9TB01095E.
[15] A. Efimov, C. Dagallier, C. Frochot, B. Myrzakhmetov, P. Arnoux, T. Heinonen, M. Mannerström, T. Toimela, Z. Ahmed, J.F. Audibert, B. Habermeyer, S. Mordon, R.B. Pansu, Photodiagnosis Photodyn. Ther. 45 (2024) 103978, https://doi.org/10.1016/j.pdpdt.2024.103978.
[16] P. Dharmaratne, B. Wang, R.C.H. Wong, B.C.L. Chan, K.-M. Lau, M.-R. Ke, C.B. S. Lau, D.K.P. Ng, K.-P. Fung, M. Ip, Emerg, Microbes Infect. 9 (1) (2020) 1628–1637, https://doi.org/10.1080/22221751.2020.1790305.
[17] C. María Curieses Andrés,, J. Manuel Pérez de la Lastra,, C. Andrés Juan,, F. J. Plou,, E. Pérez-Lebeña, 2024, p. .
[18] L.B. de O. de Siqueira,, A.P. dos Santos Matos,, M.R.M. da Silva,, S.R. Pinto,, R. Santos-Oliveira,, E. Ricci-Júnior, Photodiagnosis Photodyn. Ther. 39 (2022) 102896. 10.1016/j.pdpdt.2022.102896.
[19] A. Galstyan, Chem Eur J 27 (6) (2021) 1903–1920, https://doi.org/10.1002/chem.202002703.
[20] R. Fang, W. Xu, C. Yuan, D. Sun, Y. Guo, Y. Xu, A.C.S. Appl, Eng. Mater. 4 (2) (2026) 1093–1104, https://doi.org/10.1021/acsaenm.5c01164.
[21] M.L. Marin, L. Santos-Juanes, A. Arques, A.M. Amat, M.A. Miranda, Chem. Rev. 112 (3) (2012) 1710–1750, https://doi.org/10.1021/cr2000543.
[22] V. Trousil, J. Černý, R. Kořínková, M. Pummerová, V. Mikulcová, M. Herynková, J. Photochem. Photobiol. A Chem. 405 (2021) 112985, https://doi.org/10.1016/j.jphotochem.2020.112985.
[23] J.M. Vyskocil, N. Turgeon, J.G. Turgeon, C. Duchaine, Aerosol Sci. Technol. (2020) 1471–1478, https://doi.org/10.1080/02786826.2020.1790495.
[24] N. Turgeon, M.J. Toulouse, B. Martel, S. Moineau, C. Duchaine, Appl. Environ. Microbiol. 80 (14) (2014) 4242–4250, https://doi.org/10.1128/AEM.00767-14.
[25] R. Dey, E. Dlusskaya, N.J. Ashbolt, J. Water Health (2021), https://doi.org/10.2166/WH.2021.167.
[26] A. Fedorenko, M. Grinberg, T. Orevi, N. Kashtan, Sci. Rep. 10 (1) (2020) 22419, https://doi.org/10.1038/s41598-020-79625-z.
[27] G. Franke, B. Knobling, F.H. Brill, B. Becker, E.M. Klupp, C. Belmar Campos, S. Pfefferle, M. Lütgehetmann, J.K. Knobloch, Journal of Hospital Infection 112 (2021) 108–113, https://doi.org/10.1016/j.jhin.2021.04.007.
[28] J. Heffron,, M. Samsami,, S. Juedemann,, J. Lavin,, S. Tavakoli Nick,, B.A. Kieke,, B.K. Mayer, Water Res. 252 (2024) 121242. 10.1016/j.watres.2024.121242.
[29] L. Guo, R. Xu, L. Gou, Z. Liu, Y. Zhao, D. Liu, L. Zhang, H. Chen, M.G. Kong, Appl. Environ. Microbiol. 84 (2018) 17, https://doi.org/10.1128/AEM.00726-18.
[30] M. Ordon,, P. Nawrotek,, X. Stachurska,, M. Mizielińska, Coatings 2021, Vol. 11, Page 1179 11(10) (2021) 1179. 10.3390/COATINGS11101179.
[31] F. Pop, J. Humphreys, J. Schwarz, L. Brown, A. van den Berg, D.B. Amabilino, New J. Chem. 43 (15) (2019) 5783–5790, https://doi.org/10.1039/C9NJ01074B.
[32] M. Beran, A. Horna, V. Vorisek, E. Berkova, R. Korinkova, V. Trousil, M. Hrubanova, J. Plant Biotechnol. 49 (3) (2022) 257–270, https://doi.org/10.5010/JPB.2022.49.3.257.
[33] P. Bazant, I. Kuritka, O. Hudecek, M. Machovsky, M. Mrlik, T. Sedlacek, Polym. Compos. 35 (1) (2014) 19–26, https://doi.org/10.1002/pc.22629.
[34] H.A. Essawy,, N.A. Abd El-Wahab,, M.A. Abd El-Ghaffar, Polym. Degrad. Stab. 93 (8) (2008) 1472–8. 10.1016/j.polymdegradstab.2008.05.015.
[35] I.M. Deleanu, E. Grosu, A. Ficai, L.M. Ditu, L. Motelica, O.-C. Oprea, G. Gradisteanu Pircalabioru, M. Sonmez, C. Busuioc, R. Ciocoiu, V.I. Antoniac, Polymers (basel) 16 (21) (2024) 3028, https://doi.org/10.3390/polym16213028.
[36] N.B. Colthup, L.H. Daly, S.E. Wiberley, Introduction to infrared and Raman spectroscopy, Academic Press, 1990.
[37] B.C. Smith, Fundamentals of Fourier Transform Infrared Spectroscopy, CRC Press, 2011.
[38] M. Pittol, D. Tomacheski, D.N. Simões, V.F. Ribeiro, R.M.C. Santana, Mater. Res. 20 (5) (2017) 1266–1273, https://doi.org/10.1590/1980-5373-mr-2017-0137.
[39] N. Tkachenko, V. Golovanov, A. Penni, S. Vesamäki, M.R. Ajayakumar, A. Muranaka, N. Kobayashi, A. Efimov, Phys. Chem. Chem. Phys. 26 (26) (2024) 18113–18128, https://doi.org/10.1039/D4CP01564A.
[40] J. Wu, X. Shi, Z. Wang, F. Song, W. Gao, S. Liu, Polymers (basel). 11 (12) (2019) 1940, https://doi.org/10.3390/polym11121940.
[41] M. Furutani, M. Matsui, J. Photopolym. Sci. Technol. 38 (3) (2025) 169–172, https://doi.org/10.2494/photopolymer.38.169.
[42] N. Rouabah,, R. Nazir,, Y. Djaballah,, A.Q. Mir,, I. Ameur,, O. Beldjebli, Iranian Journal of Catalysis 13(1) (2023) 23–34. 10.30495/IJC.2023.1970800.1968.
[43] H.A. Nel, A.J. Chetwynd, C.A. Kelly, C. Stark, E. Valsami-Jones, S. Krause, I. Lynch, Environ. Sci. Technol. 55 (13) (2021) 8721–8729, https://doi.org/10.1021/acs.est.1c01085.
[44] S. Altarawneh, M. Al-Harahsheh, C. Dodds, A. Buttress, S. Kingman, Thermochim Acta 707 (2022) 179105, https://doi.org/10.1016/j.tca.2021.179105.
[45] M.C. Sin, I.K.P. Tan, M.S.M. Annuar, S.N. Gan, Polym. Degrad. Stab. 97 (11) (2012) 2118–2127, https://doi.org/10.1016/j.polymdegradstab.2012.08.020.
[46] T. Rijavec, Acta Chim. Slov. 67(4) (2020) 993–1013. 10.17344/acsi.2020.6479.
[47] B. Bouchoul, M.T. Benaniba, V. Massardier, J. Vinyl Add. Tech. 20 (4) (2014) 260–267, https://doi.org/10.1002/vnl.21356.
[48] S. Das, K. Khubdikar, Chem. Data Collect. 19 (2019) 100175, https://doi.org/10.1016/j.cdc.2018.100175.
[49] P.J.P. de Mesquita,, C.J. de F. Braz,, T.S. Alves,, R. Barbosa, Polímeros 34(1) (2024). 10.1590/0104-1428.20230100.
[50] K. McCann, B. Knudsen, R. Ananthoji, J.J. Perry, B. Hilker, M.J. Zaworotko, J. P. Harmon, J. Nanosci. Nanotechnol. 10 (9) (2010) 5557–5569, https://doi.org/10.1166/jnn.2010.2498.
[51] B. Guo, Y. He, Y. Chen, T. Yang, C. Peng, W. Luo, B. Zeng, Y. Xu, L. Dai, Nanomicro Lett. 17 (1) (2025) 116, https://doi.org/10.1007/s40820-025-01646-y.
[52] F. Mutlu, M. Pişkin, E. Canpolat, Ö.F. Öztürk, J. Mol. Struct. 1201 (2020) 127169, https://doi.org/10.1016/j.molstruc.2019.127169.
[53] S. Mapukata, J. Britton, O.L. Osifeko, T. Nyokong, Photodiagnosis Photodyn. Ther. 33 (2021) 102100, https://doi.org/10.1016/j.pdpdt.2020.102100.
[54] F. Sperandio, Y.-Y. Huang, M. Hamblin, Recent Pat. Antiinfect. Drug Discov. 8 (2) (2013) 108–120, https://doi.org/10.2174/1574891X113089990012.
[55] A. Minnock,, D.I. Vernon,, J. Schofield,, J. Griffiths,, J. Howard Parish,, S.B. Brown, J. Photochem. Photobiol. B 32(3) (1996) 159–64. 10.1016/1011-1344(95)07148-2.
[56] M. Beran, R. Korinkova, H. Polaskova, J. Drahorad, O. Vltavsky, Journal of Scientific and Engineering Research 6 (2) (2019) 44–56.
[57] L. Zeng, M.-D. Wang, S.-L. Ming, G.-L. Li, P.-W. Yu, Y.-L. Qi, D.-W. Jiang, G.-Y. Yang, J. Wang, B.-B. Chu, Redox Biol. 36 (2020) 101601, https://doi.org/10.1016/j.redox.2020.101601.
[58] J.E. Schneider, T. Tabatabaie, L. Maidt, R.H. Smith, X. Nguyen, Q. Pye, R.A. Floyd, Photochem. Photobiol. 67 (3) (1998) 350–357, https://doi.org/10.1111/j.1751-1097.1998.tb05209.x.
[59] Á. Serrano-Aroca, Int. J. Mol. Sci. 23 (10) (2022) 5335, https://doi.org/10.3390/ijms23105335.

[60] M. Qiu, Y. Chen, Y. Chu, S. Song, N. Yang, J. Gao, Z. Wu, Antiviral Res. 100 (1) (2013) 44–53, https://doi.org/10.1016/j.antiviral.2013.07.001.
[61] R. Cheng,, Y. Zhang,, T. Zhang,, F. Hou,, X. Cao,, L. Shi,, P. Jiang,, X. Zheng,, J. Wang, Frontiers of Environmental Science & Engineering 2022 16:8 16(8) (2022) 1–10. 10.1007/S11783-022-1529-4.
[62] CDC and ICAN, Best Practices for Environmental Cleaning in Healthcare Facilities in Resource-Limited Settings. Centers for Disease Control and Prevention (CDC); Infection Control Africa Network (ICAN). Available at: https://www.cdc.gov/healthcare-associated-infections/media/pdfs/environmental-cleaning-rls-508.pdf?utm. Accessed May 6, 2026.